USCAP

www.nature.com/labinvest

TECHNICAL REPORT

A novel human endometrial epithelial cell line for modeling gynecological diseases and for drug screening

Youngran Park[1], Jin-Gyoung Jung[1], Zheng-Cheng Yu[1], Ryoichi Asaka[1], Wenjing Shen[2], Yeh Wang[1], Wei-Hung Jung[4], Alicja Tomaszewski[2], Geoff Shimberg[1], Yun Chen[4], Vamsi Parimi[1], Stephanie Gaillard[2,3], Ie-Ming Shih[1,2,3]✉ and Tian-Li Wang[1,2,3]✉

Endometrium-related malignancies including uterine endometrioid carcinoma, ovarian clear cell carcinoma and ovarian endometrioid carcinoma are major types of gynecologic cancer, claiming more than 13,000 women's lives annually in the United States. In vitro cell models that recapitulate "normal" endometrial epithelial cells and their malignant counterparts are critically needed to facilitate the studies of pathogenesis in endometrium-related carcinomas. To achieve this objective, we have established a human endometrial epithelial cell line, hEM3, through immortalization and clonal selection from a primary human endometrium culture. hEM3 exhibits stable growth in vitro without senescence. hEM3 expresses protein markers characteristic of the endometrial epithelium, and they include PAX8, EpCAM, cytokeratin 7/8, and ER. hEM3 does not harbor pathogenic germline mutations in genes involving DNA mismatch repair (MMR) or homologous repair (HR) pathways. Despite its unlimited capacity of in vitro proliferation, hEM3 cells are not transformed, as they are not tumorigenic in immunocompromised mice. The cell line is amenable for gene editing, and we have established several gene-specific knockout clones targeting *ARID1A*, a tumor suppressor gene involved in the SWI/SNF chromatin remodeling. Drug screening demonstrates that both HDAC inhibitor and PARP inhibitor are effective in targeting cells with *ARID1A* deletion. Together, our data support the potential of hEM3 as a cell line model for studying the pathobiology of endometrium-related diseases and for developing effective precision therapies.

Laboratory Investigation (2021) 101:1505–1512; https://doi.org/10.1038/s41374-021-00624-3

INTRODUCTION

The human endometrium lining the inner wall of the uterus is a dynamic reproductive tissue, characterized by monthly menstrual cycle of proliferation, differentiation, and degeneration under hormonal effects. The frequent cycling of endometrial cells during a woman's lifespan, and the potential exposure to external and internal environmental factors including pathogens, environmental toxins, reactive oxygen species and hormones, make the tissue of the endometrium highly susceptible to pathogenic alterations causally associated with diseases including endometrium-related carcinomas and endometriosis [1, 2]. Indeed, endometrioid carcinoma (EMC) and clear cell carcinoma (CCC) are two major histological types of gynecological malignancies arising from the epithelial cell population of the endometrium and may present in either the uterus or ovary [3, 4]. The risk of developing ovarian EMC or CCC is strongly associated with the presence of ovarian endometriosis (endometriotic cysts) in women [5, 6]; therefore, understanding the pathogenic events leading to endometriosis may lead to a better understanding of the mechanisms promoting endometrial carcinogenesis.

Endometriosis is a benign pelvic disease, often associated with inflammatory features. It is characterized by the presence of endometrial glandular tissues outside of the uterine cavity, known as ectopic endometrial implants. The endometrial implant tissues could grow on the surface or deep into pelvic and abdominal organs and soft tissues, causing pain, infertility, tissue adhesion and fibrosis [7]. Genome-wide sequencing studies have demonstrated that glandular epithelial cells of endometriosis harbor low frequency somatic mutations in *KRAS*, *ARID1A*, or *PIK3CA* [8]. Although the mutations seen in endometriosis are non-clonal and affect only a small fraction of the glandular epithelial cells, the same types of mutations are often found in EMC and CCC and precancerous lesions, providing evidence supporting that endometriosis-associated gynecological carcinomas may originate from glandular epithelial cells [7].

Although EMC, CCC, and endometriosis affect a significant number of women, currently there are limited numbers of cell line models that can faithfully recapitulate the pathophysiology of these diseases, particularly at the precursor stage. Culturing endometrial epithelial cells in vitro has proven to be challenging. Only a few short-term primary cultured endometrial epithelial cells have been reported [9–11], and there is a lack of endometrial cell lines with stable phenotypes similar to the cell line established by Kyo et al. [12]. The development of additional representative endometrial cell lines will allow for studies aiming at better understanding the intrinsic and environmental factors that promote endometrial carcinogenesis and development of endometriosis, and provide a relevant and convenient model to test

[1]Department of Pathology, Johns Hopkins University School of Medicine, Baltimore, MD, USA. [2]Department of Gynecology and Obstetrics, Johns Hopkins University School of Medicine, Baltimore, MD, USA. [3]Department of Oncology, Johns Hopkins University School of Medicine, Baltimore, MD, USA. [4]Department of Mechanical Engineering, Johns Hopkins University, Baltimore, MD, USA. ✉email: ishih@jhmi.edu; tlw@jhmi.edu

Received: 16 February 2021 Accepted: 25 May 2021
Published online: 10 August 2021

preventative and therapeutic approaches for these diseases affecting women's health.

MATERIALS AND METHODS

Dissociation and isolation of human endometrial epithelial cells

Anonymous human endometrium tissue specimens were obtained from the Department of Pathology at the Johns Hopkins Hospital. To isolate the human endometrial epithelium, endometrium tissue was carefully dissected under a stereo-microscope (Motic, K-400, Causeway Bay, Hong Kong). Tissue fragments were minced and digested with 1 mg/ml collagenase type IV (Invitrogen) at 37° for 30 min followed by 0.25% trypsin (Invitrogen) at 37° for 10 min. To remove connective tissues and large cell masses, dissociated cells were filtered through a 40 μm nylon cell strainer (Fisher Scientific, Waltham, MA) and seeded onto a 0.1% gelatin-coated 96 well plate for clonal selection in RPMI 1640 medium supplemented with 15% fetal bovine serum (Sigma-Aldrich), 1% penicillin/streptomycin, 2 μg/ml Insulin, 1× Non-Essential Amino Acids Solution (Invitrogen), 10 ng/ml epidermal growth factor (EGF, BD Biosciences, San Jose, CA), and 200 nM 17β-estradiol (E2, Sigma-Aldrich). To generate immortalized cell lines, the cells were transduced with lentivirus bearing SV40-TAg for 48 h. Approximately one week following lentivirus infection, epithelial cells were clonally selected by morphological examination for a typical cobblestone-like shape; selected clones were subjected to further characterization (see below).

Cell viability assay

Three thousand cells were seeded in each well of a 96-well plate. After 24 h, cells were treated with various concentrations of the indicated drugs. Each treatment condition was replicated in at least five different cell wells. Cell viability was measured 24–72 h later using the CellTiter-Glo Assay kit (Promega) according to the manufacturer's instruction. Data collected at 72 h was normalized to data collected at 24 h.

Clonogenic survival assay

Cell clones from hEM3, MCF-10a, and HCT116 ARID1A-KO/WT were plated at 100–1000 cells/well. They were incubated with various concentrations of the indicated drugs. Cells were harvested after 10-14 days, fixed with 4% paraformaldehyde and stained with crystal violet. Images were acquired on a ChemiDoc Imaging System (Bio-Rad)

Western blot analysis

Ice-cold RIPA buffer (50 mM Tris-HCl pH7.4, 150 mM NaCl, 1% NP-40, 0.5% sodium deoxycholate) was used to prepare the cell lysates with freshly added 1× Halt protease inhibitor (Thermo Scientific). The lysates were centrifuged at 14,000 rpm for 15 min at 4 °C, and the supernatants were separated by 4–15% SDS-PAGE, and transferred onto a PVDF membrane using a semi-dry transfer system (Bio-Rad, Hercules, CA). Membranes were blocked with 2% non-fat dry milk and incubated with antibodies specific for EpCAM and ER (Millipore, Burlington, MA), PAX8 (Proteintech, Chicago, IL), cytokeratin 8 (CK8, Developmental Studies Hybridoma Bank, Iowa City, IA), and GAPDH (Cell Signaling, Beverly, MA). Membranes were washed with 0.1% TBST three times and incubated with Horseradish peroxidase-conjugated secondary antibody (Jackson Laboratories, West Grove, PA). Signals were detected with ECL reagents (GE Healthcare, Little Chalfont, UK).

Immunohistochemistry

Sections of formlain-fixed, paraffin-embedded human endometrium and mouse fallopian tube tissues were deparaffinized in xylene and rehydrated in graded alcohols. Antigen retrieval was performed using Target Retrieval Solution, pH 6.1 (DAKO, Carpinteria, CA), and endogenous peroxidase activity was blocked by incubation with 3% H_2O_2 for 15 min. Tissue sections were pre-incubated with blocking solution (DAKO Antibody Diluent, DAKO) for 30 min, followed by incubation with primary antibodies at 4 °C overnight. Primary antibodies used were: CK8 (Cat # TROMA-1; DSHB), PAX8 (Cat # 10336-1-AP; Proteintech), EpCAM (Cat # 2929; Cell Signaling) and ER (Cat # 04-227; Millipore). Immunoreactivites were detected using the EnVision+System peroxidase kit (DAKO) according to the manufacturer's protocol. Slides were counter stained with hematoxylin and mounted with Cytoseal mounting medium (Thermo Scientific).

Immunofluorescence staining

Cells were seeded onto 0.1% gelatin-coated coverslips in a six well plate, incubated for 72 h, washed with PBS, and fixed with 2% paraformaldehyde (Electron microscopy sciences, Hatfield, PA) for 5 min. Cells were either permeabilized with 0.2% Triton X-100 (Sigma) in TBS buffer for immunostaining with the anti-PAX8, anti-ER, and anti-CK7 antibodies, or were not permeabilized for immunostaining with the anti-EpCAM antibody. After 30 min treatment with blocking solution (10% Normal goat serum (Cell Signaling), 100 mM Tris-Hcl (pH 7.5), 150 mM NaCl), cells were incubated with primary antibodies for 1-2 hr. Cells were washed three times with PBS and incubated with Alexa Fluor 488 or other fluorphoe-cojugated secondary antibody for 1 h. Cells were then counter stained with 1 μg/ml DAPI (Sigma) for 10 s for nuclear labling, and visualized by a fluorescence microscope (Nikon, E800, Tokyo, Japan). Images were processed using the NIS-Elements imaging software (Nikon).

Spheroid assembling

Geltrex™ (Thermo Fisher, A1413201) was used for culturing hEM3 cell organoids. To prepare for the first layer of gel, 40 μL of the Geltrex was used to coat a 96-well glass-bottom plate (Cellvis, P96-1.5H-N) and incubated for 30 min at 37 °C. During the incubation, cell-mixing solution (2% Geltrex) was prepared in DMEM and stored at 37 °C. Next, 5×10^4 of hEM3 cells were resuspended in the cell-mixing solution and added on top of the solidified Geltrex gel layer. The culture was incubated for 4 days, allowing spheroids to form. The spheroid was then fixed in 4% PFA for further analysis, including immunostaining.

Flow cytometry

Cells were harvested with 0.025% trypsin containing 1 mM EDTA, washed twice with calcium- and magnesium-free PBS, fixed in 2% paraformaldehyde for 5 min, and permeabilized with 0.2% Triton X-100 in PBS for 5 min. Permeabilized cells were incubated with anti-PAX8, anti-CK8, and anti-EpCAM antibodies for 30 min, and further stained with Alexa-Fluor-488 secondary antibody (Cell signaling) for 30 min. The stained cells were then analyzed on a LSRII flow cytometer (Becton Dickinson, Franklin Lakes, NJ) and qunatified using the FlowJo software package (Ashalnd, OR). Cell cycle analysis was performed by fixing the cells in a 1:1 ratio of methanol: acetone mixture, treating with 2 mg/ml RNase, and staining with Propidium Iodide (Sigma-Aldrich). Data were acquired on a FACSCalibur flow cytometer (Becton Dickinson, Franklin Lakes, NJ).

β-galactosidase staining

The senescence β-galactosidase staining kit was used to detect β-galactosidase activity in cultured cells according to the manufacturer's instruction (Thermo Fisher). In brief, cells were fixed with Fixative solution for 10 min, and incubated with β-galactosidase staining solution at 37 °C overnight. Positive β-galactosidase activity, reflected by the blue color develoment, was visualized under an inverted microscope (Nikon, Tokyo, Japan).

In vivo tumorigenesis

The Johns Hopkins Animal Care and Use Committee approved all animal procedures (protocol number: M012M405 and M015M127). HEC1A and hEM3 cells (5×10^6) were injected subcutaneously into the flank of 6-week-old athymic nude mice. Tumor size was measured every five days using a caliper, and tumor volume was calculated according to the formula $0.5 \times (\text{length} \times \text{width}^2)$.

Short tandem repeat (STR) profiles of hEM3

STR analysis was performed on hEM3 by the Genetic Resources Core Facility, Johns Hopkins University, using a Promega GenePrint 10 Kit. The PCR products were electrophoresed on an ABI Prism® 3730xl Genetic Analyzer using an Internal Lane Standard 600 (Promega). Data were analyzed using GeneMapper® v 4.0 software (Applied Biosystems).

Sequence analysis of genes and SNP predisposed to cancer

DNA was isolated from cell lines using the Siemens Tissue Preparation System bead based automated method (Siemens Healthineers-Siemens

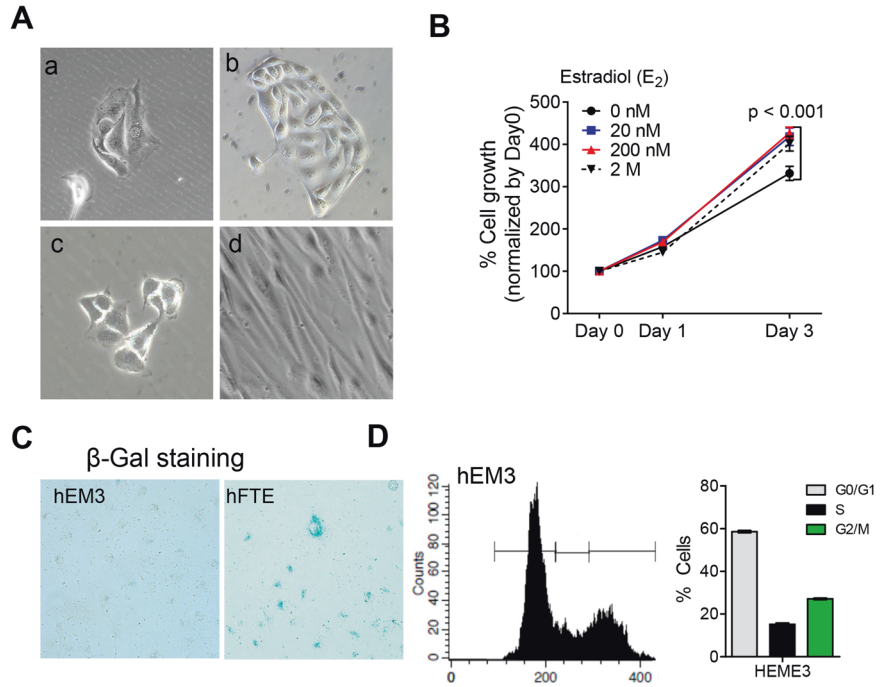

Fig. 1 Establishment and characterization of a human endometrial epithelial cell line. A Morphology of hEM3 cells at day 1 (a), day 6 (b), and 6 months (c); morphology of endometrial stromal cells (hEMS) at day 6 (d). **B** Cell growth in response to estradiol. Cells were treated with 0, 20 nM, 200 nM, or 2 μM β-estradiol. Data represent mean ± SD of four replicated wells; a multiple *t* test was performed on data collected at day 3. **C** Cellular senescence assessed by β-galactosidase staining in hEM3 cells. hEM3 cells and primary cultured human fallopian tube epithelial cells (hFTE) were stained with β-galactosidase. hFTE cells were used as a positive control for cellular senescence. **D** Cell cycle analysis of hEM3 cells. Cells were fixed with methanol/acetone and stained with Propidium Iodide (PI), followed by RNase treatment. Flow cytometric analysis of hEM3 cells (left), and the distribution of DNA contents at different cell cycle stages (right). All experiments were performed in triplicate. Data represent mean ± SD.

Medical Solutions USA, Inc). Both Qubit dsDNA HS assay (Thermal Fisher Scientific) as well as Agilent TapeStation 4200 D1000 and D1000 HS assay (Agilent) were utilized according to vendor's protocols to assess the quantity and quality of DNA isolates and sheared DNAs. NGS libraries for Illumina hybrid capture sequencing were prepared with Kapa HyperPrep reagents (Roche Sequencing). The libraries utilize IDT xGen Dual Index UMI Adapters and were hybridized to a custom 933 gene DNA based probe set from IDT. IDT xGen Hybridization blockers and Wash Kit were used to generate the final libraries (IDT-Intergrated DNA Technologies). These DNA libraries were then treated with Illumina Free adapter blocking reagent to decrease aberrant sequencing results.

Final hybrid capture libraries were sequenced on the Illumina NovaSeq using NovaSeq 6000 S1 Reagent Kit v1.5 (200 cycles) (Illumina). Sequences were aligned to the human genome reference hg19 (GRCh37). Annotation utilized the COSMIC v90 database.

An in-house custom bioinformatic pipeline (Johns Hopkins MDLVCv8) was used to process the Illumina data from the hybrid capture libraries. FASTQ files were generated from Binary Cluster Files (.bcl) using manufacturer provided demultiplexing software, bcl2fastq v2-20.0, with parameters recommended by the manufacturer. Resulting FASTQ files were aligned to the human genome reference hg19 (GRCh37) using the Burrows-Wheeler Aligner v0.7.17 algorithm with default settings. PCR duplicate marking and read pair insert size estimation was performed using Picard Tools 39 (v2.18.26). Resulting alignment files in bam and bai formats were used for further downstream processing. Variants were called using an in-house variant caller algorithm (Johns Hopkins MDLVCv8) cross referenced with HaplotypeCaller (Genome Analysis Tool Kit v3.3) under discovery mode across coding and splice sites. Variant calls passed 5% variant allele frequency filter, strand bias filter if either SB1 ≥ 0.7 and/or 2.0 ≥ SB2 ≥ 0.5 and with a minimum of 50× allele depth were retained for further analysis. Variants were annotated for genomic regions using Annovar (version 07042018) and with COSMIC (v90), gnomAD.v2.3.4 and dbSNP to know possible somatic and germline status. Variant calls falling in non-coding regions were excluded from the analysis. Further variants that are designated with dbSNP common polymorphism status or failing laboratory quality control such as a pool of normals artifact threshold were excluded from the analysis. The resulting final variant calls were confirmed by manual inspection with the integrative genomics viewer (IGV v2.3.4).

Statistical analysis

Prism 5 software package (GraphPad) was used for statistical analyses. A two-tailed Student's *t* test was used for comparing two groups. All results represent at least three independent replications, and data were shown as mean value ± SD. $p < 0.05$ was considered statistically significant.

RESULTS AND DISCUSSION

Establishment and characterization of a human endometrial epithelial cell model

In order to establish a cell model derived from endometrial epithelium, we have isolated epithelial cells which were subsequently transduced with SV40-LTAg lentivirus to inhibit replicative senescence. Approximately 1 week after lentiviral infection, we performed limiting dilutions to select individual cell clones. Single clones exhibiting epithelial "cobblestone-like" morphology were selected for further characterization (Fig. 1A). Cell clones with a "fibroblast-like" morphology were also identified and designated as endometrial stromal cells (hEMS).

One of the epithelial-like clones, hEM3, has been continuously passaged and cultured for more than five years. Cell cycle distribution of hEM3 was established by staining cells with Propidium Iodide (PI) and assessing DNA contents using flow cytometry. A homogenous cell cycle distribution pattern, a well-established characteristic of cell lines, was observed in hEM3 cells (Fig. 1D). To determine whether hEM3 cells express tissue lineage-specific markers characteristic of endometrial epithelium, we determined whether hEM3 expressed PAX8, EpCAM, cytokeratin 8 (CK8), and estrogen receptor (ER). As controls, expression levels of PAX8, EpCAM, and CK8 were evaluated on human endometrium

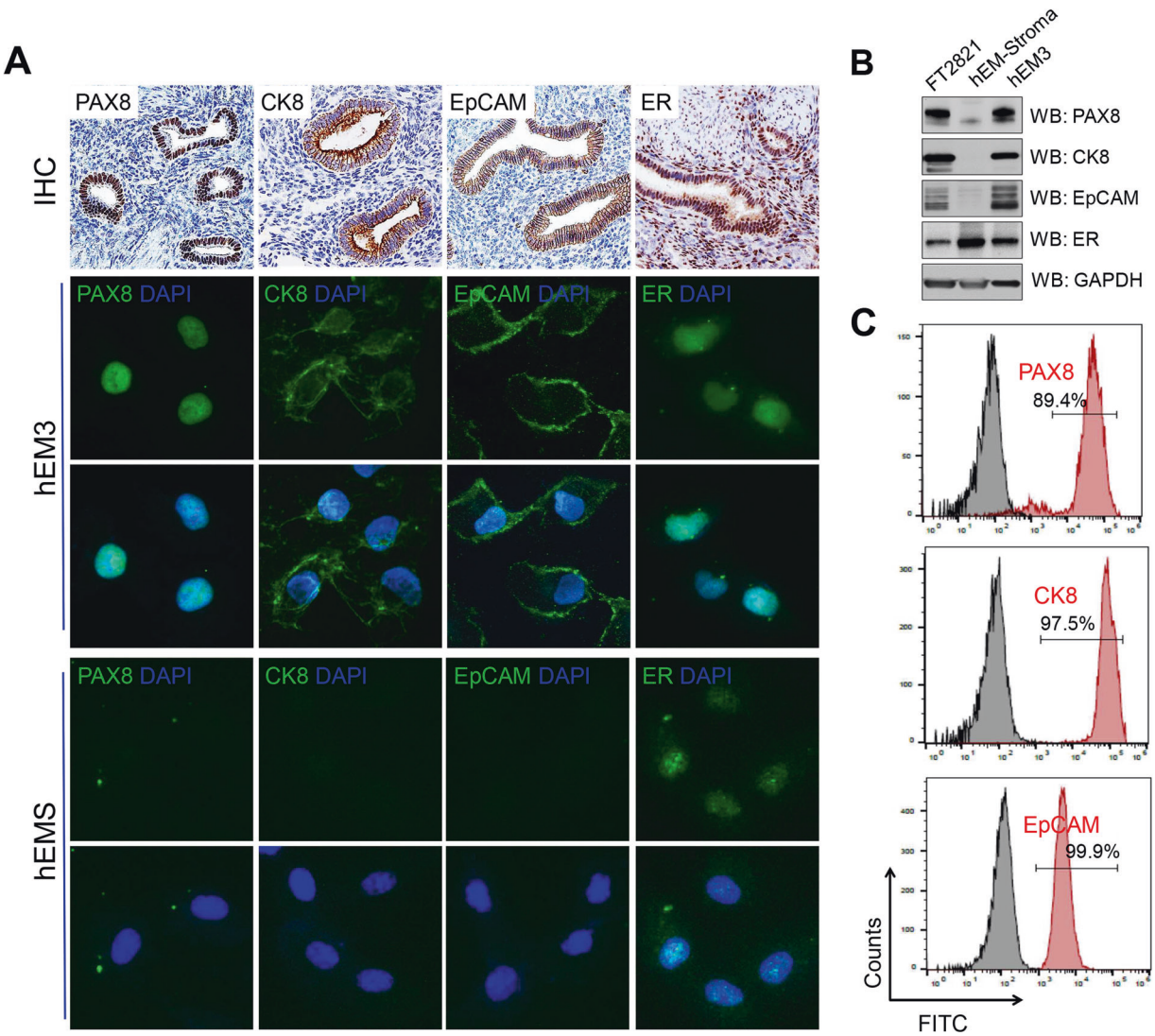

Fig. 2 Characterization of the human endometrial epithelial hEM3 cell line. A Immunohistochemistry and immunofluorescent staining of PAX8, cytokeratin 8 (CK8), EpCAM, and estrogen receptor (ER) on human endometrium (top), hEM3 cells (middle), and hEMS cells (bottom). **B** Western blot analysis of hEM3 and hEMS cells. Expressions of PAX8, CK8, EpCAM, and ER were measured in hEM3 and hEMS(troma) cells; human fallopian tube epithelial cell line, FT2821, was used as a positive control. **C**. PAX8, CK8, and EpCAM markers were evaluated in hEM3 cells by immunofluorescence staining and flow cytometry. hEM3 stained with secondary antibody was used as the control (gray area).

tissue. We found that both hEM3 cells and the endometrial epithelium were positive for expression of all these markers, whereas hEMS cells and stromal components of endometrial tissue were negative for these markers (Fig. 2A). Western blot analysis was performed to confirm protein expression of these markers in hEM3 and absence of their expression in hEMS (Fig. 2B).

Flow cytometry was employed to assess the staining intensity and population distribution. PAX8, CK8, and EpCAM-staining groups were clearly shifted to higher intensity of FITC signal (X-axis) in hEM3 cells, and 89.4%, 97.5%, and 99.9% of cell population exhibited expression of PAX8, CK8, and EpCAM, respectively (Fig. 2C).

To determine whether hEM3 cells undergo senescence, cells were assessed for the senescence-associated β-galactosidase activity using a senescence β-galactosidase staining kit. Primary cell culture of human fallopian tube epithelium (hFTE) in which many cells exhibited senescence was used as a positive control (Fig. 1C right). Compared to the positive signals detected in primary hFTE cell cultures, the great majority of EM3 cells did not undergo senescence (Fig. 1C left).

hEM3 expresses estrogen receptor (ER) and forms spheroids

The endometrium characteristically expresses ER [13, 14]. Western blot expression analysis indicated that hEM3 cells expressed ER but not PR (Supplementary Fig. 1A). Because PR expression is highly dynamic and tightly regulated by estrogen [15], the lack of continuous estrogen supplementation in the hEM3 culture system may cause the downregulation of PR.

To assess the functional responsiveness of hEM3 to estrogen, hEM3 cells were incubated with three different concentrations of β-estradiol, and subsequent cell growth was quantified. Incubation with as little as 20 nM β-estradiol induced cell growth (Fig. 1B), indicating the functional integrity of estrogen receptor signaling in hEM3 cells.

We also tested whether hEM3 can form spheroids in a 3-D culture system. hEM3 cells were grown in 3D Geltrex hydrogel as described in the Methods section. Formation of spheroids was first observed after four days. Immunostaining was then performed to validate an epithelial lineage using antibodies against EpCAM and cytokeratin 7 (CK7). hEM3 spheroids retained the expression of EpCAM and CK7. The representative images are shown in Supplementary Fig. 1B.

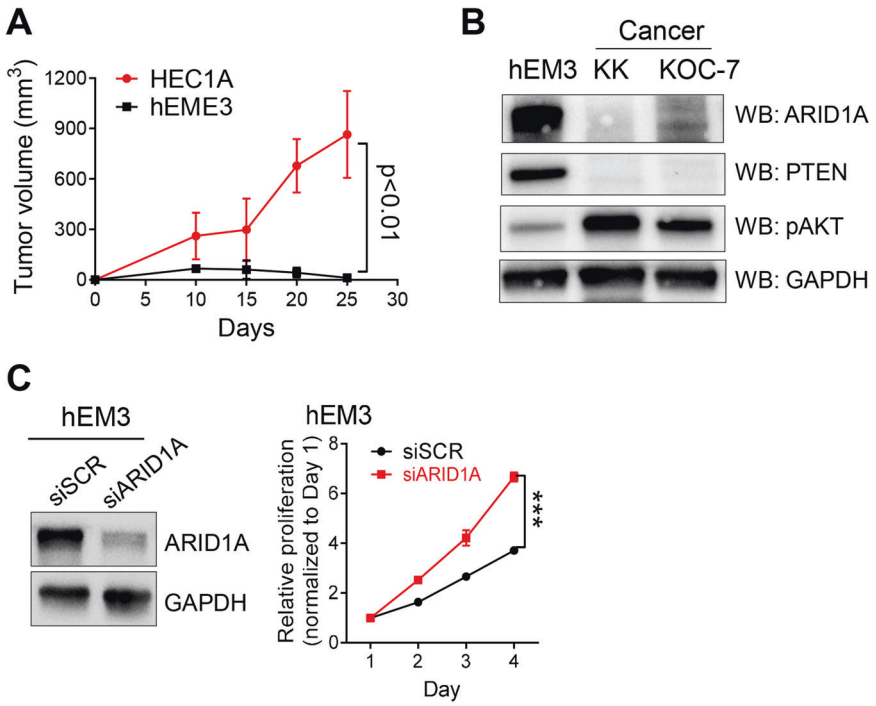

Fig. 3 Lack of tumorigenic potential in hEM3 cells. A Left; hEM3 cells did not develop tumors in athymic nude mice. hEM3 cells or HEC1A cells were injected into the flank of athymic nude mice ($n = 3$ per group). Data represent mean ± SD; $p < 0.01$, Student's t test. **B** Western blot analysis of ARID1A, PTEN, phospho-AKT, and GAPDH in hEM3, KK, and KOC-7 cells. KK and KOC-7 are ovarian CCC cell lines with minimal expression of ARID1A. **C** Left: Western blot analysis of ARID1A knockdown by siRNA in hEM3 cells. Right: Relative cell growth measured daily for 4 days. Growth results were normalized to day 1 data. Data represent mean ± SD; $p < 0.01$, Student's t test.

Karyotypic analyses were performed on hEM3 to show a near triploid karyotype with several substructural aberrations. Importantly, hEM3 cells with ARID1A knockout displayed a similar triploid karyotype and sub-chromosomal alterations as the parental hEM3 cells. Representative karyotype images are presented in Supplementary Fig. 2.

hEM3 is nontumorigenic in immunocompromised mice

Although hEM3 cells displayed unlimited proliferative activity, it was not clear whether they were tumorigenic in vivo, a hallmark of transformed cells. To test this possibility, we injected hEM3 subcutaneously into athymic *nu/nu* mice. We also performed the same experiment using the tumorigenic HEC1A endometrial cancer cell line as a positive control. HEC1A showed significant tumor growth kinetics resulting in increased end-point tumor volume as compared to the hEM3 cells (Student's t test, $p < 0.005$; Fig. 3A). hEM3 cells did not develop tumors in mice during the 4-month window of observation.

To assess whether hEM3 cells can be relevant to evaluate early tumorigenesis, we chose to study *ARID1A*. This tumor suppressor gene encoding BAF250a which is a subunit of the SWI/SNF chromatin-remodeling complex; loss-of-function mutations in *ARID1A* frequently occur in cancers derived from the endometrium [16]. ARID1A expression is detected in normal endometrium and in hEM3 cells but not in endometrioid or clear cell carcinoma cell lines including KK and KOC7, which are known to harbor loss-of-function mutations (Fig. 3B). To evaluate the effects of ARID1A inactivation in hEM3 cells, ARID1A expression was silenced by siRNA, and cell growth was measured (Fig. 3C). Similar to a previous report [17], reduction of ARID1A expression significantly enhanced proliferation in hEM3 cells as compared to hEM3 cells transfected with the scramble control siRNA.

PTEN is another tumor suppressor gene whose expression is frequently downregulated because of gene deletion, loss-of-function mutation or epigenetic silencing. Western blot analysis demonstrated that PTEN expression was detected in hEM3 cells but not in cancer cell lines, KK and KOC7, derived from endometrium-associated cancers (Fig. 3B). PTEN loss often activates downstream PI3K/AKT signaling, and we found that both KK and KOC7 cell lines but not the hEM3 upregulated pAKT, indicating that PTEN inactivation in KK and KOC7 but not in hEM3 (Fig. 3B).

hEM3 does not carry germline mutations in DNA repair genes

We performed Short Tandem Repeat (STR) profile analysis for eight STR loci to verify hEM3 genetic identify (Table 1). STR profile of hEM3 cells did not match to any STR reference profiles from human cell lines in ATCC or DSMZ databases. These results provide evidence that hEM3 is a unique cell line and its STR profile reported here establishes reference standards for future research use.

A significant fraction of endometrium-derived gynecological cancers, especially the endometrioid carcinoma, display DNA mismatch repair (MMR) deficiency due to loss-of-function mutations or DNA hypermethylation in gene(s) involving the MMR pathway. This DNA repair defect causes microsatellite locus instability (MSI) and hypermutation in the genome, making it the most comprehensively characterized (micro) genetic instability in human cancer. Germline mutations of MMR genes define Lynch Syndrome, an inherited cancer-prone phenotype associated with an increased risk of endometrial and colorectal cancers.

To determine whether hEM3 harbors pathogenic germline mutations in DNA repair genes, we applied targeted next generation sequencing method to analyze MLH1, MSH2, MSH6, PMS1 and PMS2, which participate in DNA mismatch repair, and BRCA1, BRCA2, ATM, RAD51C, RAD51D, and PALB2, which involve DNA homologous recombination repair. Pathogenic germline mutations were not identified in any of these genes, suggesting that DNA repair systems in hEM3 are relatively intact, and

therefore, can be useful for functional assessment of DNA repair genes through gene manipulation approaches such as gene knock-in or knockout.

Application of the hEM3 cell model in drug screening

The potential of utilizing hEM3 for drug screening was further explored. Specifically, we evaluated whether the inactivation of ARID1A would sensitize hEM3 to small molecule compounds targeting DNA repair or glutamine metabolism. ARID1A knockout (KO) cell clones were generated from hEM3 parental cells by double nicking, CRISPR/Cas-mediated editing as previously described [18]. Telomerase expression and activity were observed in hEM3 cells. Additionally, ARID1A-KO hEM3 cells, as compared to parental cells, had higher telomerase expression and activity as previouly reported [18]. Drug sensitivity assays were performed on additional pairs of isogenic ARID1A-KO and –WT cell lines, HCT116 and MCF-10a, that display differences in their DNA repair capacity. HCT116 is a colorectal cancer cell line which is defective in MMR DNA repair because of mutations in MLH1 and loss of MSH3 expression and is considered MSI-high [19]. MMR deficiency occurs in ~20–30% of endometrioid carcinomas (EMCA), and ARID1A loss can occur in the MMR-deficient EMCA, especially in those with high-grade features [20]. Given that there are very few MMR-deficient EMCA lines with engineered *ARID1A* deletion, HCT116 was often used as a model for investigating genetic interaction between MMR and ARID1A. On the other hand, deleterious *ARID1A* mutations are also frequently detected in human cancers without MMR deficiency [16, 21]. Human cell lines such as hEM3 and MCF-10A without MMR deficiency can be valuable reagents to investigate ARID1A function in the MMR-proficient context. MCF-10a was established from normal mammalian glands and, similar to hEM3, MCF-10a has low malignant potential and is non-tumorigenic in immunocompromised mice [22].

Drug sensitivity data obtained from the MCF-10a ARID1A-KO/WT isogenic cell line pair are generally consistent with those obtained from the hEM3 ARID1A-KO/WT cell line pair. On the other hand, the widely used HCT116 ARID1A-KO/WT cells did not have the same response. For example, both hEM3 and MCF-10a ARID1A-KO cells failed to show an increased response to the glutaminase inhibitor (GLSi), CB-839, compared to the WT cells, whereas HCT116 ARID1A-KO displayed significantly increased GLSi sensitivity compared to WT HCT116 cells (Fig. 4A, B). In contrast, both hEM3 and MCF-10a ARID1A-KO cells manifested a higher sensitivity to the WRN DNA helicase inhibitor, NSC-617145, than the WT cells whereas there was no such differential drug response in the HCT116 ARID1A-KO cells (Fig. 4C). In another example, hEM3 and MCF-10a ARID1A-KO cell clones were more sensitive to methyl methanesulfonate, an alkylating agent, when combined with PARP inhibitor, Olaparib, as compared to the ARID1A-WT cells (Fig. 4D). Interestingly, the responses to some of the drugs were consistent among these three isogenic pairs of ARID1A-KO/WT cell lines. For example, all three ARID1A-KO cell lines were more sensitive to PARP inhibitors, Olaparib and Niraparib, and to HDAC inhibitor, ACY1215, than their WT counterpart controls, the results show good agreement with previous reports [23–25].

The discrepancy observed among different cell lines may be explained by the differences in the genotype of DNA repair genes.

Table 1. STR profile.

Loci	C2
D5S818	13
D13S317	12
D7S820	10
D16S539	10, 12
vWA	13, 16
TH01	7
AMEL	X
TPOX	9, 11
CSF1PO	11, 12
D21S11	27, 28

Note: Loci with one allele listed are homozygous for that STR marker.

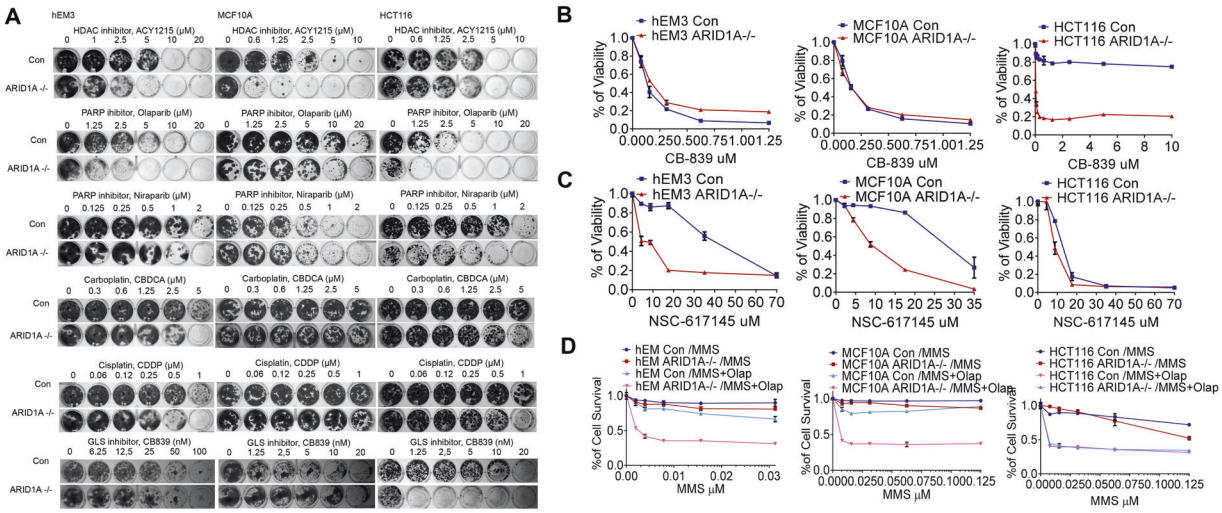

Fig. 4 Drug sensitivity test on three pairs of ARID1A-KO and WT isogenic cell lines. A In vitro colony formation assays performed on three pairs of ARID1A-KO and WT isogenic cell lines established from hEM3, MCF-10a, and HCT116. Cells were grown in media containing the indicated concentrations of HDAC inhibitor (ACY1215), PARP inhibitor (Olaparib and Niraparib), DNA cross-linker (Carboplatin and Cisplatin), and metabolic modulator (CB839). After two weeks, cell clones were stained with crystal violet for further quantification. **B** Drug response was determined using a cell proliferation assay. ARID1A-KO and WT isogenic cell lines were exposed to serial concentrations of a glutaminase inhibitor, CB839 (**B**), WRN DNA helicase inhibitor, NSC-617145 (**C**), and a combination of methyl methanesulfonate (MMS) and PARP inhibitor (**D**). Four days later, viable cells were assessed via PrestoBlue (Thermo Scientific). Data are normalized to data collected at zero drug concentration, and are presented as mean ± SD.

For example, HCT116 has mutations and functional deficiency in DNA mismatch repair, whereas the other two cell lines were derived from normal glandular epithelium without known mutations in DNA repair genes. As a result, they are more likely to faithfully respond to and repair DNA damages than cancer cells such as HCT116. Although this is our preferred view, differences in malignant potential between hEM3/MCF10a and HCT116 may also be considered. Nevertheless, the data highlight specific genotype-phenotype relationship observed in drug metabolism and treatment response. Our observation also underscores the importance of evaluating pathogenic variants in DNA repair genes or evaluating DNA repair capability in each patient-derived cell line used for small molecule or CRISPR screening. Moreover, the previously reported tumorigenic endometrial cancer cell line with deletion of *ARID1A* established from the genetically modified mouse [26] and the conditioned *ARID1A* knockout mouse uterine and ovarian tumor models [26, 27] are applicable models with MMR-proficient status for testing novel treatments for *ARID1A*-inactivated cancers.

CONCLUSION

The study presented here describes the establishment of a human endometrial epithelial cell line that biologically and functionally resembles normal human endometrial epithelium. This cell line is characterized by expression of epithelial lineage markers, ability to grow spheroids, and non-tumorigenicity in immunocompromised mice. Moreover, this endometrial cell line demonstrates high genetic and phenotypic stability, and does not have mutations in key genes in the DNA repair pathways. As a result, this cell line can be considered for drug efficacy studies or functional assays focusing on DNA repair pathways. The distinct drug response in DNA mismatch repair deficient cells compared to mismatch repair proficient endometrial cells highlights the importance of pre-evaluating the genotypes of cell models used for drug sensitivity tests or for CRISPR screening. An improved understanding of differential drug response in cell lines with distinct pathogenic mutations/polymorphisms or DNA repair capacities would help offer better precision treatment for women with endometrial diseases.

DATA AVAILABILITY STATEMENT

The authors confirm that the data supporting the findings of this study are available within the article and its supplementary materials. Raw data are available upon request.

REFERENCES

1. Chapron, C., Marcellin, L., Borghese, B. & Santulli, P. Rethinking mechanisms, diagnosis and management of endometriosis. Nat Rev Endocrinol 2019;15:666–82.
2. Setiawan VW, Yang HP, Pike MC, McCann SE, Yu H, Xiang YB, et al. Type I and II endometrial cancers: have they different risk factors? J Clin Oncol. 2013;31:2607–18.
3. Yen TT, Wang TL, Fader AN, Shih IM, Gaillard S. Molecular classification and emerging targeted therapy in endometrial cancer. Int J Gynecol Pathol. 2020;39:26–35.
4. Kurman RJ, Visvanathan K, Shih IM. Bokhman's dualistic model of endometrial carcinoma- revisited. Gynecol Oncol. 2013;129:271–272.
5. Ogawa, S., Kaku, T., Amada, S., Kobayashi, H., Hirakawa, T., Ariyoshi, K. et al. Ovarian endometriosis associated with ovarian carcinoma: a clinicopathological and immunohistochemical study. Gynecol Oncol 2000;77;298–304.
6. Wilber MA, Shih IM, Segars JH, Fader AN. Cancer implications for patients with endometriosis. Sem Reprod Med. 2017;35:110–116.
7. Wang Y, Nicholes K, Shih IM. The origin and pathogenesis of endometriosis. Annu Rev Pathol. 2020;15:71–95.
8. Anglesio MS, Papadopoulos N, Ayhan A, Nazeran TM, Noe M, Horlings HM, et al. Cancer-associated mutations in endometriosis without cancer. N Engl J Med. 2017;376:1835–48.
9. Arnold JT, Kaufman DG, Seppala M, Lessey BA. Endometrial stromal cells regulate epithelial cell growth in vitro: a new co-culture model. Hum Reprod. 2001;16:836–45.
10. Classen-Linke I, Kusche M, Knauthe R, Beier HM. Establishment of a human endometrial cell culture system and characterization of its polarized hormone responsive epithelial cells. Cell Tissue Res. 1997;287:171–85.
11. Akoum A, Doillon CJ, Koutsilieris M, Dompierre L, Maheux R, Villeneuve M, et al. Human endometrial cells cultured in a type I collagen gel. J Reprod Med. 1996;41:555–61.
12. Kyo S, Nakamura M, Kiyono T, Maida Y, Kanaya T, Tanaka M, et al. Successful immortalization of endometrial glandular cells with normal structural and functional characteristics. Am J Pathol. 2003;163:2259–69.
13. Ka H, Seo H, Choi Y, Yoo I, Han J. Endometrial response to conceptus-derived estrogen and interleukin-1beta at the time of implantation in pigs. J Anim Sci Biotechnol. 2018;9:44.
14. Geisert RD, Pratt TN, Bazer FW, Mayes JS, Watson GH. Immunocytochemical localization and changes in endometrial progestin receptor protein during the porcine oestrous cycle and early pregnancy. Reprod Fertil Dev. 1994;6:749–60.
15. Wu SP, Li R, DeMayo FJ. Progesterone receptor regulation of uterine adaptation for pregnancy. Trends Endocrinol Metab. 2018;29:481–91.
16. Jones S, Wang TL, Shih Ie M, Mao TL, Nakayama K, Roden R, et al. Frequent mutations of chromatin remodeling gene ARID1A in ovarian clear cell carcinoma. Science. 2010;330:228–31.
17. Guan B, Wang TL, Shih IM. The tumor suppressor role of ARID1A in gynecological cancer. Cancer Res. 2011;71:6718–27.
18. Suryo Rahmanto Y, Jung JG, Wu RC, Kobayashi Y, Heaphy CM, Meeker AK, et al. Inactivating ARID1A tumor suppressor enhances tert transcription and maintains telomere length in cancer cells. J Biol Chem. 2016;291:9690–9699.
19. Haugen AC, Goel A, Yamada K, Marra G, Nguyen TP, Nagasaka T, et al. Genetic instability caused by loss of MutS homologue 3 in human colorectal cancer. Cancer Res. 2008;68:8465–72.
20. Allo G, Bernardini MQ, Wu RC, Shih Ie M, Kalloger S, Pollett A, et al. ARID1A loss correlates with mismatch repair deficiency and intact p53 expression in high-grade endometrial carcinomas. Mod Pathol. 2014;27:255–61.
21. Wiegand KC, Shah SP, Al-Agha OM, Zhao Y, Tse K, Zeng T, et al. ARID1A mutations in endometriosis-associated ovarian carcinomas. N Engl J Med. 2010;363:1532–43.
22. Soule HD, Maloney TM, Wolman SR, Peterson WD Jr., Brenz R, McGrath CM, et al. Isolation and characterization of a spontaneously immortalized human breast epithelial cell line, MCF-10. Cancer Res. 1990;50:6075–86.
23. Park Y, Chui MH, Suryo Rahmanto Y, Yu ZC, Shamanna RA, Bellani MA, et al. Loss of ARID1A in tumor cells renders selective vulnerability to combined ionizing radiation and PARP inhibitor therapy. Clin Cancer Res. 2019;25:5584–94.
24. Shen J, Peng Y, Wei L, Zhang W, Yang L, Lan L, et al. ARID1A deficiency impairs the DNA damage checkpoint and sensitizes cells to PARP inhibitors. Cancer Discov. 2015;5:752–67.
25. Altucci L. A key HDAC6 dependency of ARID1A-mutated ovarian cancer. Nat Cell Biol. 2017;19:889–90.
26. Guan, B, Rahmanto, YS, Wu, RC, Wang, Y, Wang, Z, Wang, TL, et al. Roles of deletion of Arid1a, a tumor suppressor, in mouse ovarian tumorigenesis. *J Natl Cancer Inst.* 2014; 106.
27. Suryo Rahmanto Y, Shen W, Shi X, Chen X, Yu Y, Yu ZC, et al. Inactivation of Arid1a in the endometrium is associated with endometrioid tumorigenesis through transcriptional reprogramming. Nat Commun. 2020;11:2717.

ACKNOWLEDGEMENTS

The study was supported by Ovarian Cancer Research Alliance (IMS and TLW) and the Richard W. TeLinde Endowment, the Johns Hopkins University (IMS) and NIH grants, CA215483, P50CA228991 and HD096147 (IMS and TLW). YC acknowledges the support from the National Institute of Biomedical Imaging and Bioengineering [R21 EB029677, S10 OD025193]. WHJ acknowledges the support of the National Cancer Institute [F99 CA253759].

AUTHOR CONTRIBUTIONS

YP, JGJ, ZCY, RA, WS, YW conceived and performed the experiments and analyzed the data. JGJ and YP derived the cell models. AT and GS wrote the manuscript in consultation with YP, TLW, IMS, and SG. 3-D organoid cultures performed by WHJ and YC. STR genotyping and cell line karyotyping performed by VP.

COMPETING INTERESTS

The authors declare no competing interests.

ETHICAL APPROVAL

The study was approved by the institutional review board (IRB) at the Johns Hopkins University.

ADDITIONAL INFORMATION

Supplementary information The online version contains supplementary material available at https://doi.org/10.1038/s41374-021-00624-3.

Correspondence and requests for materials should be addressed to I.-M.S. or T.-L.W.